Adapted GMR Array used in Magnetic Flux Leakage Inspection

Marc KREUTZBRUCK, Andreas NEUBAUER, Matthias PELKNER, Verena REIMUND

BAM Federal Institute for Materials Research and Testing, Division 8.4,
Unter den Eichen 87, 12205 Berlin, Germany, marc.kreutzbruck@bam.de

Abstract

GMR sensors are increasingly used for magnetic surface inspection due to their high sensitivity and high spatial resolution. In case of simple planar or cylindrical shaped components, the GMR-based inspection procedure can be automated easily. In order to reduce the inspection time we present a GMR-based NDT-system consisting of a yoke and a coil as a local magnetization unit. This way the global magnetization step and, if necessary, the corresponding demagnetization cycle can be avoided reducing the number of working steps. Using a local probe we measured plates, bearings, and rails, each of which containing real fatigue cracks and reference artificial cracks of different depths and orientations. Cracks with a depth of 40 µm could be resolved with a signal-to-noise ratio of about 20. A reduction of the measuring time can be obtained using a sensor array. We present an optimized sensor array for nondestructive testing application, where gradiometric arranged GMR layers were fabricated on a board with up to 48 GMR sensors. Each sensor detects the vertical field gradient. In our example the baseline was chosen to be 250 µm which efficiently suppress external background fields without losing sensitivity for the detection of surface breaking defects.

Keywords: Flux Leakage Testing, GMR-Sensors, Sensor Arrays

1. Introduction

Magnetic flux leakage testing (MFL) is one of the most popular method for defect detection and characterization of ferromagnetic components in NDT. An example for a MFL application is the magnetic particle inspection (MP). In this method magnetic particles accumulate at magnetic stray fields generated in the vicinity of surface cracks in a magnetized component being under examination. By means of MP the number of defects and their length can be determined precisely, however, the estimation of the defect depth is not feasible and automation of MP-applications is rather difficult. To examine the depth and width of inhomogeneities in more detail it is useful to measure the stray field near cracks, which can be performed by any magnetic field sensor, such as flux gate sensors, hall probes, SQUID or XMR sensors (magneto resistance; X = G (giant), A (anisotropic), etc) [1-5].

GMR sensors are well suited for NDT applications thanks to their high sensitivity, high signal-to-noise ratio and small sensing area associated with a high spatial resolution. In contrast to commercial GMR sensors embedded into bulky encapsulation the GMR sensors used here were adapted in a way that its sensitive layers are located only a few 10 µm from the chip edge, resulting in a small sensor-to-surface distance and thus better SNR and spatial resolution. This supports the approach to compare the measured data with a fast inverse scheme based on a semi-analytic model for MFL, enabling us to estimate the defect parameters like width, length and depth.

2. Detection of Surface Breaking Cracks

Usually a GMR sensor exists of four elements fabricated as a Wheatstone-bridge, resulting in an output signal with a distinct reduction of temperature dependence. Every two elements are positioned at the same place and both areas are separated by a certain distance. Such a configuration is called gradiometer and can be seen in Fig. 1. The measured quantity is the difference of the magnetic field (here the normal component) between the two active areas and can be detected by measuring the bridge voltage. Our gradiometer has sensing areas with a size of only 60 µm × 70 µm and provides a transfer function in the order of about 14 mV/V · $(kA/m)^{-1}$.
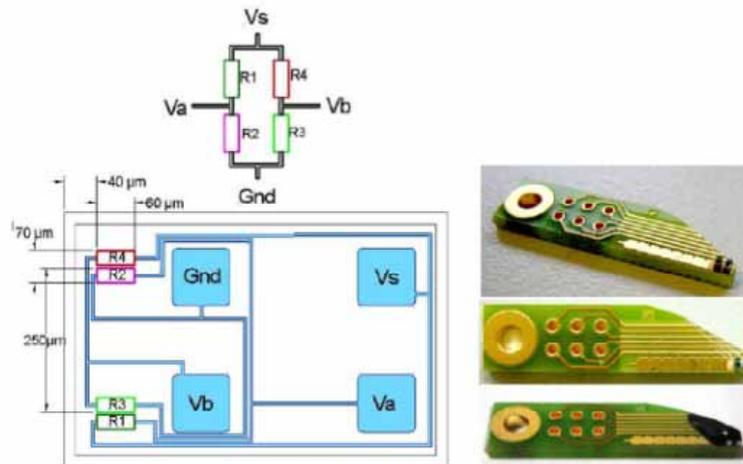

Figure 1: GMR gradiometer (*Sensitec GmbH*) measuring the tangential gradient of the normal field component for distance between the two sensing areas of 250 µm. Left: Sketch of the electronic circuit of the GMR Chip. Right: Picture of a complete GMR-device mounted on a connecting board.
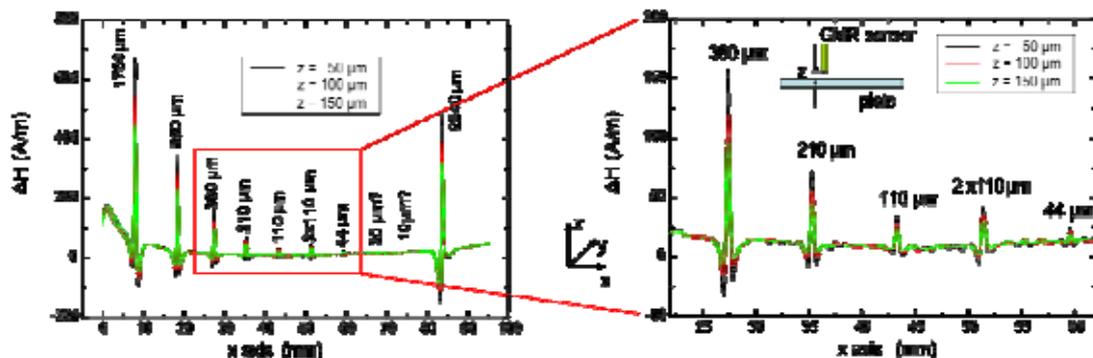

Figure 2: MFL signal for the detection of surface breaking cracks using a GMR gradiometer for three different distances *z* between sensor and surface.

As test object we used a steel plate with artificial cracks of varying depth. The artificial cracks were introduced by low energy electrical discharge machining [3]. The width varies between 100 to 200 µm and the length is about 5500 µm. The depth ranges between 10 µm up to 2240 µm. The measurements were performed in remanence (no applied field during measurement), meaning that the test object had been magnetized before. The direction of applied field was normal to the geometry of the defects.

Using the gradiometer a line scan was measured with different lift-offs. In Fig. 2 we show the magnetic field as function of the sensor position. One can observe clear signatures of the defects of different depths. For a better illustration we extract in the right panel of Fig.2

the signals for the defect with depths ranging between 44 µm and 380 µm. The attenuation of the signal strength for an increasing sensor-to-surface separation is in agreement with the theoretical model. It can be seen that even the 44 µm-deep defect can be distinguished from the noise originating from the material itself. This noise could either be caused by the roughness of the surface or by the spatial variation of the permeability.

3. Local Magnetization Unit

In order to save the required magnetization step we used a local magnetization unit directly embedded in the probe. The design of the local magnetization unit was supported by 3D-FE simulations (Opera,VectorFields), as shown in Fig. 3 (a, b). The experimentally investigated magnetic material properties of the bearing were taken into account. The relative maximum non-linear permeabilities of the yoke and bearing are $\mu_y \approx 2800$ and $\mu_b \approx 96$, respectively. The yoke has a width of 10.2 mm, which allows the implementation of a sensor array, and a pole distance of 10 mm. The air-gap between yoke and bearing is 100 µm. A DC current of 1A driving the coil (N=100) yields a simulated applied field $H_a = 817$A/m in the roller bearing (100 µm below the surface) at the center of the yoke, shown in Fig. 3 (b). Towards the sides of the yoke the applied field continuously decreases to $H_a = 602$ A/m, as indicated by the red dots. The prototype probe was constructed following the specifications given above. A single GMR sensor (GF792, Sensitec), used as a magnetometer in a half-bridge setup, was positioned in the center of the yoke, measuring the normal magnetic field component H_z. This sensor was adapted for NDT applications, i.e., the sensitive layer has a size of only 20 x 17 μm^2 and it is positioned at the edge of the sensor, allowing a reduced sensor-to-surface distance of about 100 µm. The linear part of the response function of the sensor is 6.1 (mV/V)(kA/m).

An area scan of the roller bearing containing artificial surface cracks is shown in Fig. 3 (c). For clarity we depict only the positive field amplitudes of the normal field component H_z. Distinct signatures of the straight cracks are clearly visible. For the artificial crack with a depth of only 40 µm a sufficient signal to noise ratio of at least 10 dB is obtained. In the case of the rotated crack (45°) the magnetic stray fields are still detectable. However, since these signals are only slightly above the largest background signals further signal processing is desirable for a distinct detection. The signals shown were corrected for a constant background field which is present due to a slightly off-centered sensor position.
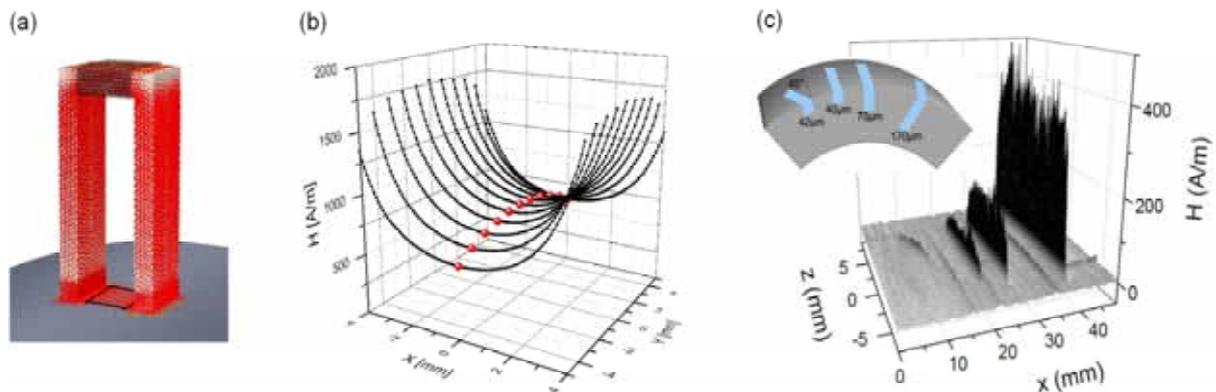

Figure 3. (a) FE simulation (OPERA) of the magnetic yoke. The black square indicates the area for which H_a was evaluated at 100 µm below the surface, as shown in panel (b). (c) Measured MFL area scan across four artificial defects. The inset schematically illustrates the artificial cracks realized with low energy spark erosion [3]. They are characterized by a constant width of 93 µm and a length of several mm. The depths are 40 µm, 70 µm, and 170 µm, as well as 42 µm for the rotated (45°) crack.

4. Detection of Subsurface Defects

We also investigated several samples which are used for the containment of spent nuclear fuel for long-time storage. The containers are made of nodular cast iron suitable for magnetic inspection. The measurements were carried out using a local magnetization unit for magnetizing the testing object. The yoke of the local magnetization unit has a width of 18 mm and each of the two coils (N = 100) was driven with a current $I = 1.2$ A. For ferromagnetic objects with a relative permeability of $\mu = 80$, simulations give an applied field of about $H_a = 800$ A/m in the center of the yoke and 100 µm below the surface of the testing object. The sensor array was positioned at the center of the yoke. The surfaces were scanned using a high precision positioning stage with a resolution around 1µm. The sensor-to-surface distance was around 100 µm. Along the x-direction data were recorded equally spaced every 16 µm. In y-direction data were recorded every 200 µm. The scans were carried out at a speed of 40 mm/s (along the x-direction). A reduction of the scanning velocity did not affect the measurement results. In principle higher scanning velocities are possible.
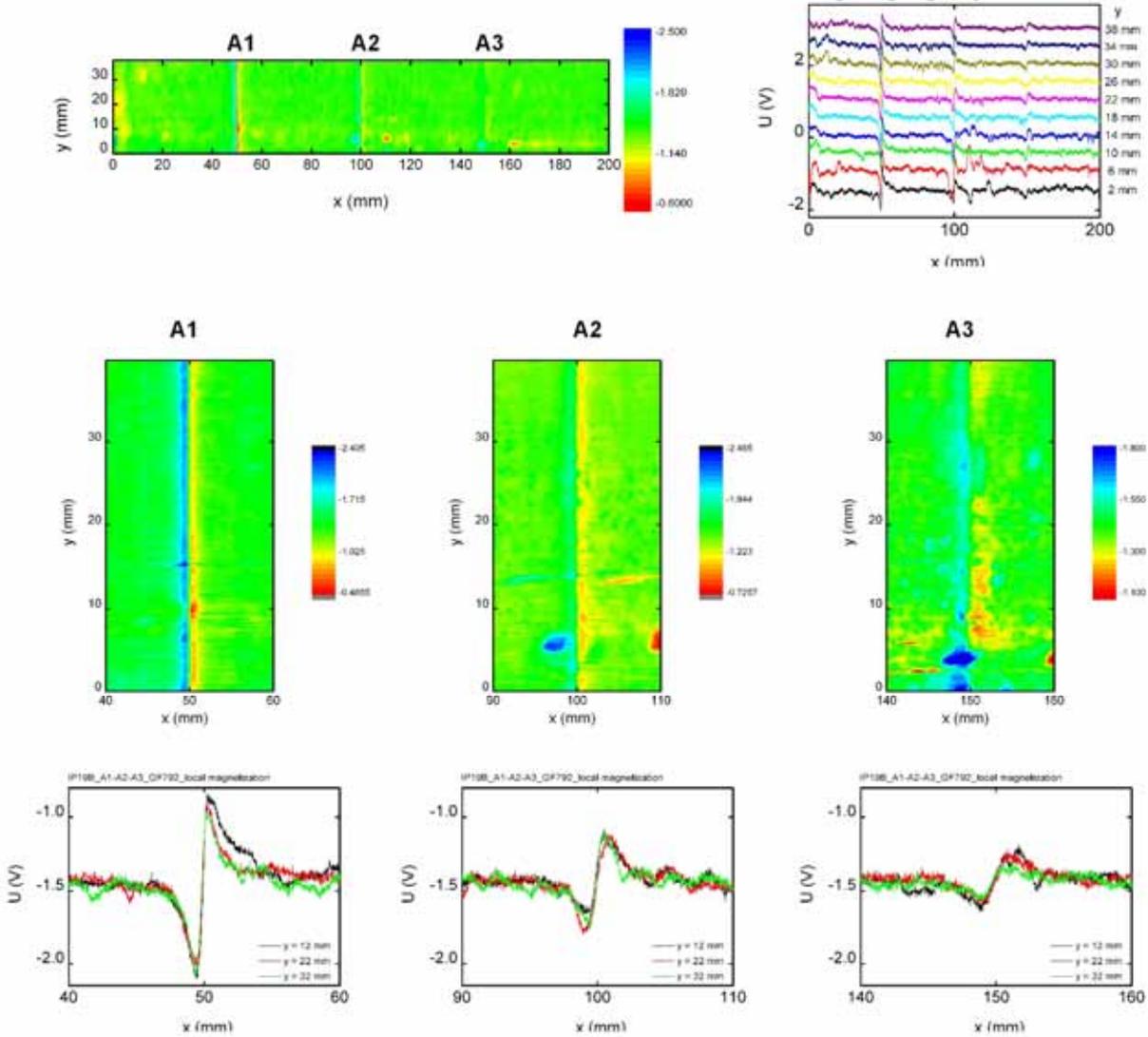

Figure 4: An area of 200 x 39 mm² was scanned. Defect A1 (250 µm ligament) and A2 (500 µm ligament) are clearly visible. Also defect A3 (1000 µm ligament) is visible, although it is partly on the boarder of giving a clear signal. There are lines with a signal-to-noise (SNR) ratio of more than 10 dB, as well as lines with a SNR below 6 dB.

The reference sample contains 3 hidden defects each of which having a defect height of 2.5 mm, a length of 8 mm and an opening of 350 µm. The ligaments are 0.25 mm (A1), 0.5 mm (A2), and 1mm (A3). The defects are detectable with different signal-to-noise ratios. A1 could be detected with an SNR of 25 dB, A2 was detected with an SNR of 17 dB and A3 with a typical SNR of about 12 dB (see also Fig. 4).

For the presented results no filters (analog or digital) were applied and no image processing was carried out. This should further reduce of the background noise and, hence, improve the testing results. Also the magnetic and mechanical testing procedure was not appropriate adapted to this testing problem. For example, the magnetic yokes used for this investigation were constructed for use on polished surfaces. Hence, the rough surface of the testing objects lead to an enhanced background noise due to the friction of the magnetic yokes. This means that an optimization of the design of the yoke (shape, magnetic field strength and guidance) results in a reduction of the background noise and an enhancement of the defect signal.

5. Detection of Fatigue Surface Cracks

Fig. 5 shows a grey scaled plot of real roll contact fatigue cracks, which mainly occur in curved rails (Fig. 5, right). The depth of these cracks can be up to several mm. For the measurement the test specimen was magnetized before, hence, the residual field inside the material was exploited. As shown in Fig. 5, left all cracks could be detected with a high resolution using GMR sensors. However, the internal field inside the material is difficult to determine. Demagnetization effects depending on the geometry lead to a reduction of the field inside the material, particularly at the edges of the test specimen. For this reason, an evaluation of the cracks is complicated. In addition, diversifying background fields caused by the object itself play a role, i.e., they can saturate the GMR sensor in the worst case. In this respect a local magnetization may be advantageous since it leads to a constant background field and allows controlling the internal field distribution. A good understanding of the internal field is important to benchmark the signals in terms of defect geometry.
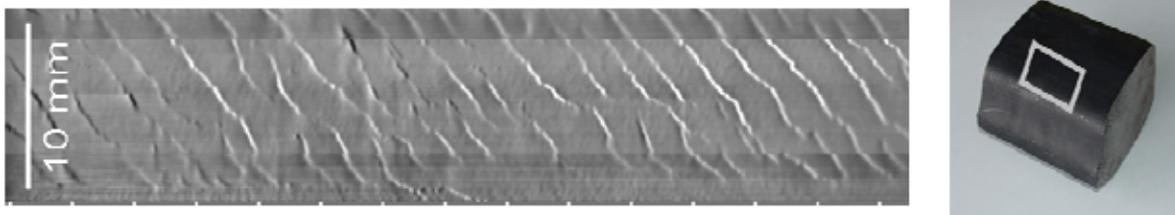

Figure 5. Left: GMR measurement of roll contact fatigue cracks of rails. Right: Test specimen; the squared box marks the scanned area.

6. NDT-adapted GMR Sensor Arrays

The previous measurements were mainly carried out with prototypes of different single GMR sensors that were adapted to the needs of MFL testing through a reduction of the sensor-to-surface distance by means of mechanical grinding. After achieving positive results with these sensors, we designed sensor arrays with up to 16 sensors per chip which then were manufactured on 5-inch silicon wafers. Due to both physical and production-oriented reasons a gradiometric setup measuring the field gradient $\partial H_z/\partial z$ normal to the surface was chosen for these sensor arrays. In order to optimize the alignment and geometry of the active sensor

layers to the needs of MFL testing, an elaborate parameter study was carried out (not published so far). The resulting sensor arrays thus differ from the alignment and position of the GMR surfaces used in section 2 (Fig. 1), where we measured the lateral field gradient $\partial H_x/\partial x$ parallel to the surface under test.

Figure 6 shows two different layouts of the GMR sensor arrays (top) as well as their manufactured counterparts (bottom). In (a) an array of 8 sensors with a length of 400 µm each and in (b) an array of 16 sensors with a length of 200 µm of each single sensor is shown. The effective measurement width of both sensor arrays is 3.4 mm. Figure 6 (c) shows two of these sensor arrays mounted on a prototype circuit board, again especially designed for MFL-testing. Care was taken to obtain a minimal distance between the active sensor layers and the edge of the circuit board, since it allows for a minimization of the sensor-to-surface distance which is essential for MFL-testing of microcracks.

In order to achieve the testing velocities necessary for industrial applications, we currently designed a board housing 48 GMR sensors with a total width of 10.2 mm (see Fig. 6 (c)), with three sensor arrays of 16 sensors each. The data will be quasi-simultaneously read out via a fast multiplex electronics. This enables us to achieve a testing velocity of around 1 m/s, while maintaining resonable sample rates with a corresponding step size of below 50 µm.
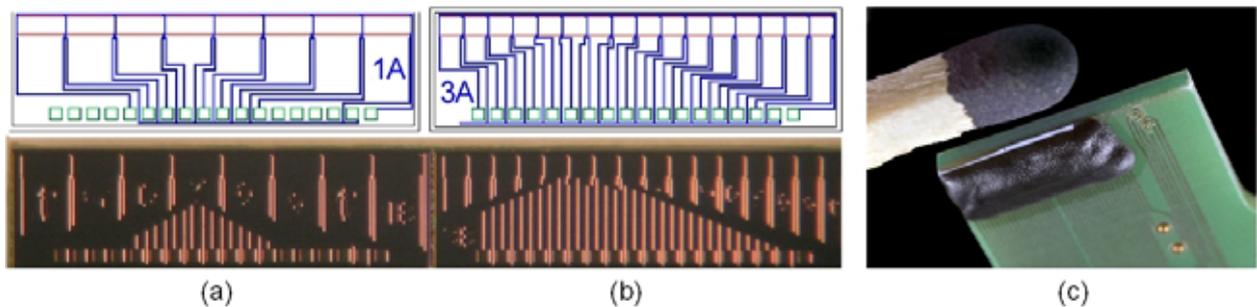

Figure 6: Layout (top) and manufactured GMR sensor array (bottom) consisting of (a) 8 and (b) 16 GMR-layer structures in a gradiometric set-up. The voltage signals are read out via a half-bridge setup with reference resistors. (c) Image of a prototype measuring board holding two sensor arrays (below the black shielding).

We inspected again the cylinder roller bearing, which was already introduced in Fig. 3c, showing the four artificial cracks with depths of 42 µm (45° rotated defect), 40 µm, 70 µm (length 8 mm), and 170 µm (length 13 mm). The crack opening (gap) was about 95 µm.

In this example we used the array providing 16 single gradiometer elements, each of which consisting of two GMR active surfaces which are separated from each other in a vertical distance of 250 µm (baseline of the gradiometer). The size of the GMR area is determined by the lateral length and the height which was 190 µm and 0.6 µm, respectively. The latter is significantly smaller than the lateral size taking into account that stray fields decay distinctly for increasing distance between surface and sensor. The separation of each sample point was in the order of 30 µm and the amplification factor was in the order of 40 dB for each channel.

In Fig. 7a we observe a relative flat response, which changes within the interval 540 mm $< x <$ 580 mm, where we introduced the low energy EDM-notches. The deepest crack (170 µm) causes a peak-to-peak stray field signal strength of 1400 A/m (somewhat more than 1 mT), whereas the smallest crack signal is about 180 A/m caused by the 42 µm deep crack which was rotated by 45° (Fig. 7b). The latter leads to a remarkable SNR of about 12, assuming a noise level of about 15 A/m, resulting in. The 40 µm, the 70 µm and the 170µm deep cracks show an peak-to-peak amplitude of about 300 A/m, 800 A/m, and 1400 A/m, respectively, leading to an SNR of up to 90. The fact that such little crack depth can be detected with these high SNR-values can be explained by both the low distance between the

surface and the sensor array of below 100µm and the small sensing area. Besides the good SNR this also leads to a high spatial resolution. In Fig. 7c we observe a distance between the maxima and minima of below 200 µm and a width of the signature below 500 µm. This will help also to detect defects which are very close to each other.

Fig. 7e shows a picture of the GMR probe without encapsulation including the GMR board, the yoke, the mechanical mounting and the bearing under test. In this testing concept we operate the system in direct contact to the rotating sample. For this purpose we used a probe with 3 wheels made from steel. The contact wheels cause no magnetic influences or any mechanical and vibration caused noise contributions. This concept helps to better control the distance between the sensor and the sample under test compared to non-contact solutions.
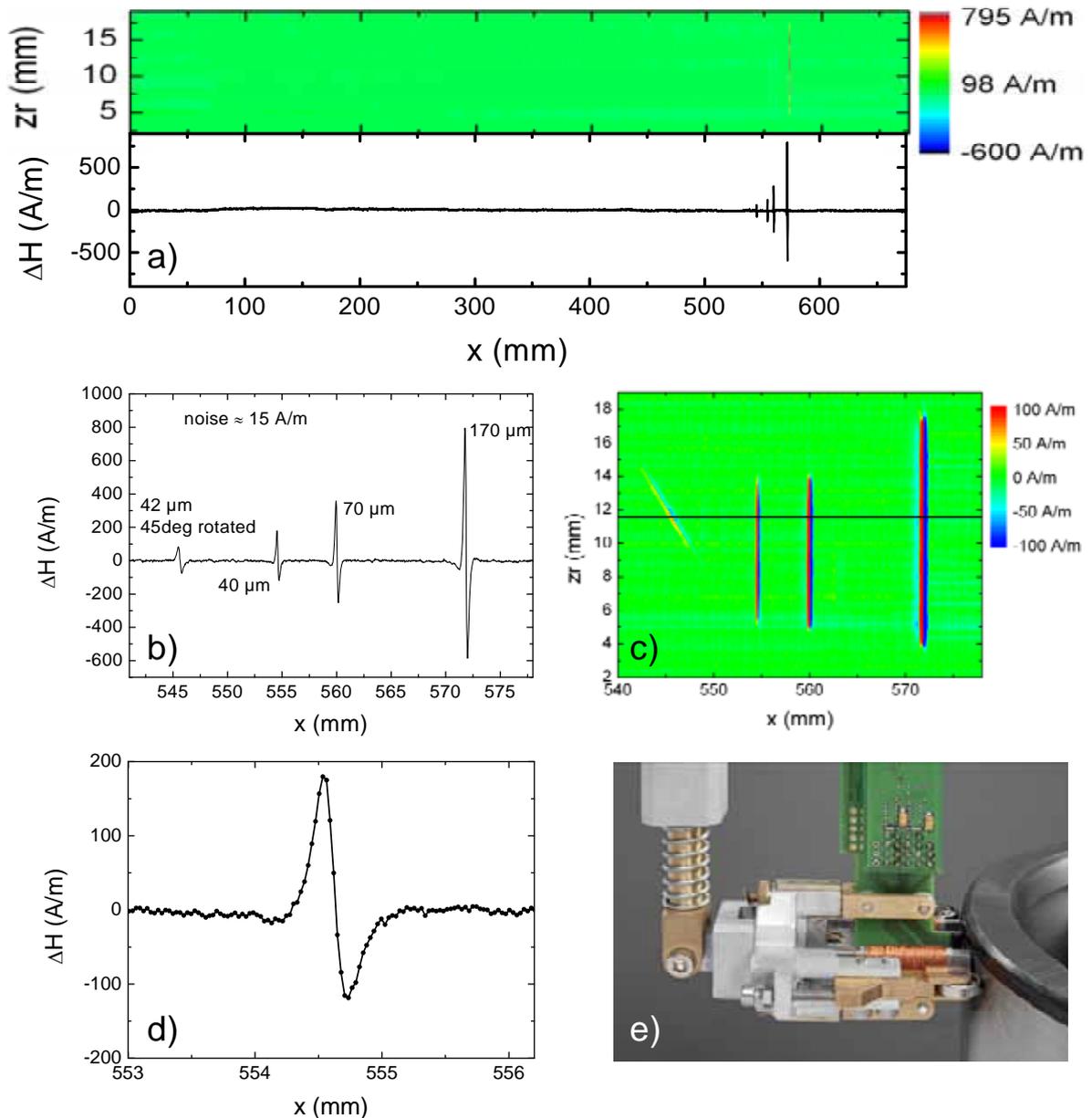

Figure 7: a) Vertical field component $\partial H_z/\partial z$ as function of the position above the total outer surface of the bearing (false color representation from 0° to 360 ° and a line scan at $z_r = 11.5$ mm). b) Vertical field component $\partial H_z/\partial z$ along the line ranging from $x = 540$ mm to $x = 580$ mm at $z_r = 11.5$ mm. c) A-scan of the magnified area $(540 < x < 580, 2 < z_r < 19)$ mm in false color representation. d) Zoom of the signal of the 40µm deep crack at $x = 554.5$ mm. e) Photograph of the GMR probe without encapsulation including the GMR board, the yoke, the mechanical mounting and the bearing under test.

7. Conclusion

In the presented paper we demonstrated a reliable detection of artificial and real fatigue cracks using an adapted GMR sensor design. Using a single GMR sensor within a gradiometric design a 44 µm deep crack was resolved with a SNR better than 6 without subsequent filtering of the signals (see also [6]). Also hidden defects with ligaments of up to 1 mm were detected within cast iron samples. Having a further reconstruction and the reliable description of the defect geometry in mind, the knowledge of the magnetic field distribution inside a magnetic specimen is essential [7]. In order to reliably describe the generation of the applied fields –and also for practical reasons to prevent the global magnetization step– the internal field was locally excited by a yoke-like magnetization unit.

Since the GMR can be miniaturized, active sensing layers of only a few µm² area are possible. Hereby, the step into micro-NDT detecting small cracks is available. The results show that GMR sensors can also be used for an automated NDT-process. This is especially the case for simple geometries in which the mechanical handling of the probe can meet the requirements of positioning accuracy in terms of Lift-off, tilting angles and vibration. For this purpose sensor arrays of a few ten and more elements are preferable to reduce measuring time leading to a reduction of the inspection costs for NDT industries. In section 6 we showed the fabrication of NDT-adapted GMR arrays, which can detect even a very small crack depth with high SNR. The lateral size of the sensors determines then the total scanning time and the sensitivity for the detection of a certain defect size.

For a multi-channel approach one has to consider that in MFL we do not need very high sample rates in the upper MHz-regime and thus low cost multiplexing concepts can be used in order to set up a dime a dozen multi channel read-out electronics. Furthermore, besides the optimization of the detection probability, the high sensitivity and good spatial resolution properties of GMR sensors support the defect shape reconstruction approach. Here, an almost "point-like" pick up characterization of the magnetic field sensor is advantageous to achieve sound reconstruction results. The future focus is here to set up inverse algorithms to gain quantitative information and thus provide in comparison to conventional MPI (magnetic particle inspection) a deeper insight into the degree of damage. The latter is a significant improvement when it comes to fracture mechanical life time estimations or to feed back capabilities to improve the control of production parameter.

References

[1]   J.-T. Jeng, G.-S. Lee, W.-C. Liao, and C.-L. Shu. *J. Magn. Magn. Mater.*, **304**, pp. e470-e473 (2006)

[3]   K. Allweins, M. von Kreutzbruck, and G. Gierelt, *J. Appl. Phys.* **97**, 10Q102 (2005)

[2]   T. Dogaru and S. T. Smith, IEEE *Trans. Magn.* **37**, pp. 3831-3838 (2001).

[3]   A. Tamburrino, S. Ventre, L. Ferrigno, and S. Udpa, *Int. J. Appl. Electrmagn. Mech.*, **28**, pp. 329-336 (2008)

[4]   Y. Kataoka, S. Murayama, H. Wakiwaka, and O. Shinoura, *Int. J. Appl. Electrmagn. Mech.*, **15**, pp. 47-52 (2001/2002).

[5]   M. Pelkner, M. Blome, V. Reimund, H.-M. Thomas, and M. Kreutzbruck, "Flux leakage measurements for defect characterization using a high precision 3-axial GMR magnetic sensor" in *Review of Progress in QNDE,* **30A**, edited by D. O. Thompson and D. E. Chimenti, AIP Conference Proceedings vol. 1335, (2010), pp. 380-387.

[6]   M. Pelkner, A. Neubauer, M. Blome, V. Reimund, H.-M. Thomas, M. Kreutzbruck, *Studies in Applied Electromagnetics and Mechanics* IOS Press, Vol.35, 217-224 (2011)

[7]   M. Kreutzbruck, K. Allweins, C. Strackbein, H. Bernau, *International Journal of applied electromagnetics and mechanics,* **30**(3,4), 299-308, 2009